Supporting Information

The coordinated film-formation dynamics by intermediate state engineering enables efficiently thickness-insensitive organic solar cells

Xin Song[1,6]*, Hao Xu[1], Xinyu Jiang[2], Shengzheng Gao[1], Xinjie Zhou[1], Shanlei Xu[1], Junjun Li[3], Jian Yu[3], Wenzhu Liu[4], Weiguo Zhu[1]*, Peter Müller-Buschbaum[2,5]

1: School of Materials Science and Engineering, Jiangsu Engineering Laboratory of Light-Electricity-Heat Energy-Converting Materials and Applications, Changzhou University, Changzhou 213164, P. R. China

2: Chair for Functional Materials, Department of Physics, TUM School of Natural Sciences, Technical University of Munich, James-Franck-Str. 1, 85748 Garching, Germany

3: School of New Energy and Materials, Southwest Petroleum University, Chengdu 610500, P. R. China

4: Research Center for New Energy Technology, Shanghai Institute of Microsystem and Information Technology, Chinese Academy of Sciences, Shanghai 201800, P. R. China

5: Heinz Maier-Leibnitz-Zentrum, Technical University of Munich, 85748 Garching, Germany

6: Key Laboratory of Advanced Energy Materials Chemistry (Ministry of Education), Nankai University, Tianjin 300071, P. R. China

*Correspondence: xin.song@cczu.edu.cn, zhuwg18@126.com

1. Materials

PM6 was purchased from Solarmer Materials Inc. Y6, PY-IT, BTR-Cl was purchased from Dethon Optoelectronics Materials Inc. LTD. L8-BO and PNDI-F3N-Br were purchased from Nanjing Zhiyan Inc. LTD. Poly(3,4-ethylenedioxythiophene):poly(styrenesulfonate) (PEDOT:PSS) PEDOT:PSS, Baytron P VP Al 4083 from H. C. Starck was commercially available from Heraeus (Germany). 1, 3,5-tribromobenzene (TBr) was purchased from Sigma. All materials and solvents were commercially available and used as received.

2. Devices Fabrication

The devices were fabricated with conventional structures of ITO/PEDOT:PSS/BHJ/PNDI-F3N-Br/Ag(100 nm). The patterned ITO glass substrates (SuZhou ShangYang Solar Technology Co., Ltd.) were cleaned sequentially under sonication with deionized water and isopropanol, and then dried at 60 ℃ in a baking oven overnight. After UV-ozone treatment for 15 min, a PEDOT:PSS layer (~40 nm) was spin-coated on ITO substrate at 4800 rpm for 30 s, and then baked in air at 150 °C for 15 min; Sequentially, the active layer solution of PM6:Y6 (1:1.2, chloroform, 18 mg/ml) was spin-coated at 3000 rpm for 30 s. For TBr treatment, TBr was firstly dissolved in chloroform solvent with a concentration of 15 mg/ml. After 20 min stirring at room temperature, this TBr solution was used as solvent and added to the PM6:Y6 mixture to form PM6:Y6:TBr solution (18 mg/ml). After stirring overnight, the blend solution was directly spin-coated at 3000 rpm on the PEDOT:PSS treated ITO

substrates with thermal annealing treatment at 85 °C for 5 mins. After that, PFNDI-F3N-Br methanol solution with a concentration of 0.5 mg mL^{-1} was spin-coated on the active layer at 2000 rpm for 30 s. To complete the fabrication of the devices, 100 nm of Ag was thermally evaporated through a mask under a vacuum of ~5×10^{-4} mbar. The active area of the devices was 0.06 cm^2. For PM6:L8-BO, 15 mg/ml TBr was dissolved in chloroform to form the TBr solution. After 20 min stirring at room temperature, this TBr solution was added to the PM6:L8-BO mixture to form the PM6:L8-BO:TBr (18 mg/ml) solution. After stirring overnight, the blend solution was directly spin-coated at 3000 rpm for 30s on the PEDOT:PSS treated ITO substrates with a thermal annealing treatment at 85 °C for 5 mins. After that, PFNDI-F3N-Br methanol solution with a concentration of 0.5 mg mL^{-1} was spin-coated on the active layer at 2000 rpm for 30 s. To complete the fabrication of the devices, 100 nm of Ag was thermally evaporated through a mask under a vacuum of ~5×10^{-4} mbar.

3. Device characterizations

***J-V* and EQE**

The photovoltaic performance was measured under an AM 1.5G spectrum from a solar simulator (Newport) with an active are of 0.06 cm^2. The illuminated are with a mask is 0.568 cm^2. The current density-voltage (J-V) characteristics were recorded with a Keithley 2400 source meter with a range from −0.2 to 1.2 V with a scan step of 50 mV and a dwell time of 10 ms. The light intensity of the light source was calibrated before the testing by using a standard silicon (Si) solar cell, as calibrated by a National Renewable Energy Laboratory (NREL) certified silicon photodiode, giving a value of

100 mW/cm^2. The external quantum efficiency (EQE) spectra were obtained on a commercial EQE measurement system (Taiwan, Enlitech, QE-R3011). The light intensity at each wavelength was calibrated by a standard single-crystal Si photovoltaic cell. Highly sensitive EQE was conducted by an integrated system with Fourier transform photocurrent meter (PECT-600, Enlitech).

Density Functional Theory (DFT) Calculations

DFT for geometry optimizations and electronic properties was calculated by B3LYP-D3BJ functional with 6-31G** basis at Gaussian09 package. [1] The geometries were visualized through GaussView5.0[2] and VMD[3] software. All possible structures of each complex were generated by the Molclus software [4], and each of the generated structures was then fully optimized by DFT calculations to obtain the respective total energy and locate the most stable geometry for each complex. These stable geometries did not show any imaginary frequency in normal mode analysis, which revealed that these complexes were true minima on the potential energy surfaces. Among these, the minimum energy structure was selected as the most feasible structure for further analysis. In addition, to determine the attractive and repulsive interaction contributions, the reduced density gradient analysis was performed using MultiWfn3.6 software. [5]

Space-Charge-Limited-Current (SCLC) Measurement

Hole-only and electron-only devices were fabricated to measure corresponding mobilities of active layers by using the space charge limited current (SCLC) method with structure of ITO/PEDOT:PSS/active layer/MoO_3/Ag and ITO/ZnO/active layer/ZnO/Ag, respectively. Here, the preparation of active layer was consistent with

that of the photovoltaic devices. The mobilities (μ) were determined by fitting the dark current to the model of a single carrier SCLC, described by the equation:

$$J = \frac{9}{8} \varepsilon_0 \varepsilon_r \mu \frac{V^2}{d^3}$$

where J is the current, E is the effective electric field, ε_0 is the permittivity of free space, ε_r is the material relative permittivity, d is the thickness of the active layer, and V is the effective voltage. The effective voltage was obtained by subtracting the built-in voltage (V_{bi}, the built-in voltage due to the relative work function difference of the two electrodes) and the voltage drop (V_s, due to contact resistance and series resistance across the electrodes) from the applied voltage (V_{appl}), $V = V_{appl} - V_{bi} - V_s$ The mobility was calculated from the slope of the $J_{1/2}$-V curves. The thickness of the BHJ blend for SCLC measurement was about 90 nm.

Atomic Force Microscopy

Tapping-mode atomic force microscopy (AFM) images were obtained using a NanoScope NS3A system (Digital Instrument).

UV-vis Absorption Measurement

UV-vis absorption spectra were recorded on a Shimadzu spectrophotometer.

Time-Resolved Photoluminescence

TR-PL was performed at Fluo Time 300 Fluorescence Lifetime Spectrometer.

Transient Photocurrent and Photovoltage

In the TPC, Photo-CELIV and TPV measurements, the OSCs were fabricated with the same method as mentioned above. The data were obtained by the all-in-one characterization platform, Paios (Fluxim AG, Switzerland).

Deep level transient spectroscopy

The transient current response is analyzed by applying a negative voltage of -3V to the device in the dark. Using the following equation to estimate the defect distributions in organic semiconductors. Considering the dependence of carrier transport position in the device, the current peak in the first 0.1μs is mainly caused by the displacement current, so the fitting of 0.1 ~ 100μs at room temperature are dominant. The trapped defect state volume density Nt of the discrete energy trap can be expressed as:

$$j_{te}(t) = \frac{1}{\tau_{te}} \cdot q \cdot d \cdot N_t \cdot exp(-\frac{t}{\tau_{te}})$$

Where $j_{te}(t)$ is trap emission current, τ_{te} is catch-trap emission time constant, q is a single charge amount, d is the film thickness of the device, N_t is the trap state density.

Laser Confocal Raman Microspectroscopy

Raman mapping were measured by LabRAM XploRA (HORIBA Jobin Yvon). PM6 possesses a characteristic Raman peak at 2955 cm^{-1}, and Y6 has a characteristic position at 2212 cm^{-1}.

FT-IR Characterization

FT-IR spectra were recorded on a PerkinElmer, Spectrum 100.

XPS Characterization

The XPS measurements were carried out on an ESCALAB 250Xi spectrometer (Thermo Scientific, USA) equipped with a pass energy of 30 eV with a power of 100 W (10 kV and 10 mA) and a mono-chromatized AlKα X-ray (hν=1486.65 eV) source. All samples were analyzed under a pressure of less than 1.0×10^-9 Pa. Spectra were acquired through the avantage software (Version 5.979) with a step of 0.05 eV.

GIWAXS Characterization

The GIWAXS data were collected with a SAXSLAB laboratory beamline using a CuKα X-ray source (8.05 keV, 1.54 Å) and a Pilatus 300K detector. The incident angle was 0.2° for the GIWAXS measurements. The sample-to-detector distance (SDD) was set to 95 mm. The transformation to q-space, radial cuts for the in-plane /out-of-plane analysis, and azimuthal cuts for orientation analysis were processed by the MATLAB-based package GIXSGUI.[6]

Film-depth-dependent light absorption spectroscopy (FLAS)

The FLAS was performed by a homemade instrument as previously reported. [7] A self-developed soft plasma source generated by glow-discharging of low-pressure oxygen

was used to incrementally etch the film without degage to the underneath films, which were in-situ monitored by a spectrometer. FLAS is extracted from the evolution of the light absorption spectra during soft plasma etching. The film-depth-dependent exciton generation is obtained upon the modified optical transmission matrix method, taking film-depth-dependent light absorption spectra and optical interference into simulation. We can obtain the photoelectric field at any position in the layer by

$$E_j(x) = (t_j^+ e^{i\xi_j x} + t_j^- e^{-i\xi_j x})E_0^+ = t_j^+ \left[e^{i\xi_j x} + r_j'' e^{i\xi_j (2d_j - x)}\right]E_0^+$$

absorption power of monochromatic light at wavelength is given by

$$Q(x,\lambda) = \frac{4\pi c\varepsilon_0 \kappa_j n_j}{2\lambda}\left|E_j(x)\right|^2 = \frac{1}{2}c\varepsilon_0 \alpha_j n_j \left|E_j(x)\right|^2$$

Exciton production rate of the active layer is given by

$$G(x) = \int_{\lambda_1}^{\lambda_2} \frac{\lambda}{hc} Q(x,\lambda)d\lambda$$

.

The detail of the optical modeling is available in the literature published by Lu et a1.[7,8]

References

[1] M. J. Frisch, G. W. Trucks, H. B. Schlegel, G. E. Scuseria, M. A. Robb, J. R. Cheeseman, G. Scalmani, V. Barone, B. Mennucci, G. A. Petersson, H. Nakatsuji, X. Li, M. Caricato, A. Marenich, J. Bloino, B. G. Janesko, R. Gomperts, B. Mennucci, J. B. Foresman, D. J. Fox, Gaussian 09, Gaussian, Inc.Wallingford, CT 2009.

[2] R. J. Dennington, T. K. Millam, GaussView 5.0, Semichem Inc., Shawnee Mission KS, 2009

[3] W. Humphrey, A. Dalke, K. Schulten, "VMD - Visual Molecular Dynamics", *Journal of Molecular Graphics*, **1996**, 14, 33-38.

[4] T. Lu, molclus program, Version 1.9.9.7, http://www.keinsci.com/research/molclus.html

[5] T. Lu, F. Chen. Multiwfn: a multifunctional wavefunction analyzer. *Journal of Computational Chemistry*, **2012,** *33*, 580-592.

[6] Z. Jiang, GIXSGUI: a MATLAB toolbox for grazing-incidence X-ray scattering data visualization and reduction, and indexing of buried three-dimensional periodic nanostructured films. *Journal of Applied Crystallography* **2015,** *48*, 917-926.

[7] Z. Wang, Y. Hu, T. Xiao, Y. Zhu, X. Chen, L. Bu, Y. Zhang, Z. Wei, B. Xu, G. Lu Correlations between performance of organic solar cells and film-depth-dependent optical and electronic variations, *Advanced Optical Materials*, **2019**, *7*, 1900152.

[8] L. Bu, M. Hu, W. Lu, Z. Wang, G. Lu, Printing Semiconductor-insulator Polymer Bilayers for High-performance Coplanar Field-effect Transistors. *Advanced Materials*, **2018,** *30*, 1704695.

Figure S1. The molecular structure of DBCl and TBr.

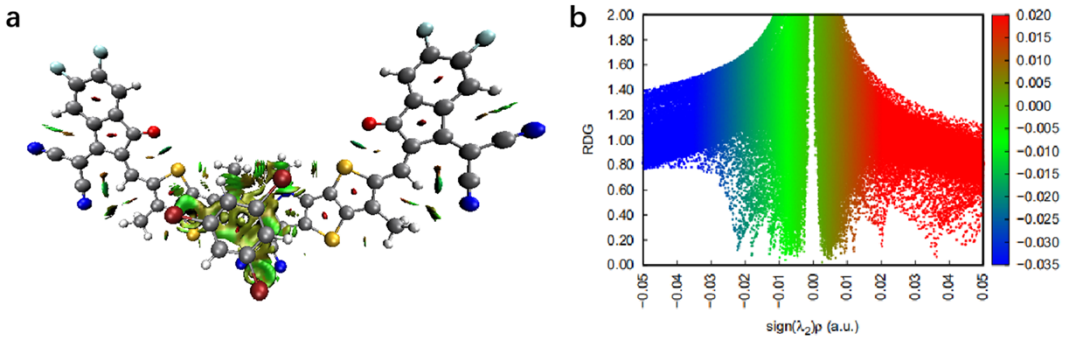

Figure S2. (a) Reduced density gradient (RDG) iso-surface map and (b) the functions of RDG and Sign $(\lambda_2)\rho$ for Y6:TBr dimer.

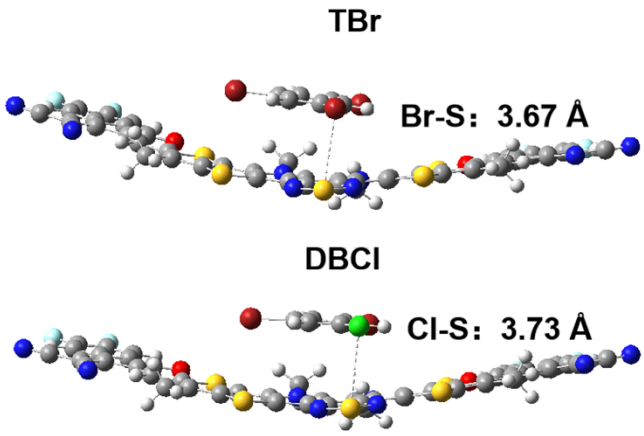

Figure S3. The distance between halogen and sulfur atoms in TBr:Y6 and DBCl:Y6.

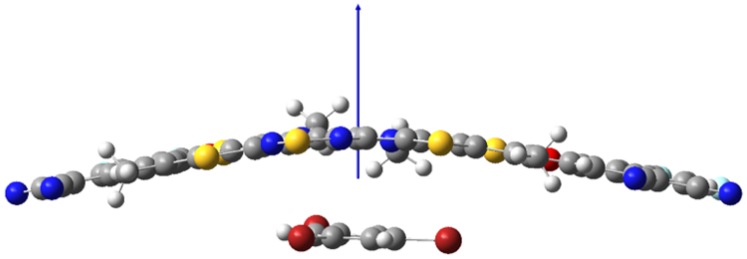

Figure S4. The dipole direction of Y6:TBr dimer.

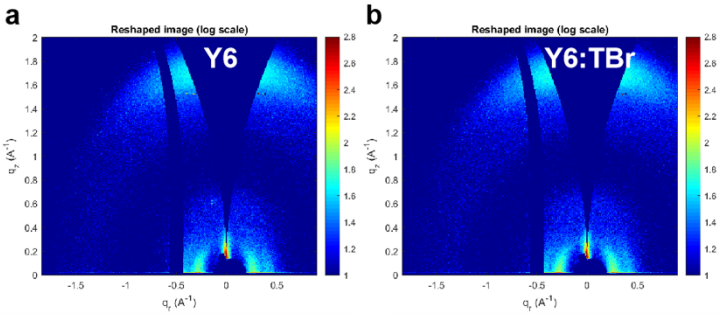

Figure S5. 2D GIWAXS data of Y6 and Y6:TBr films.

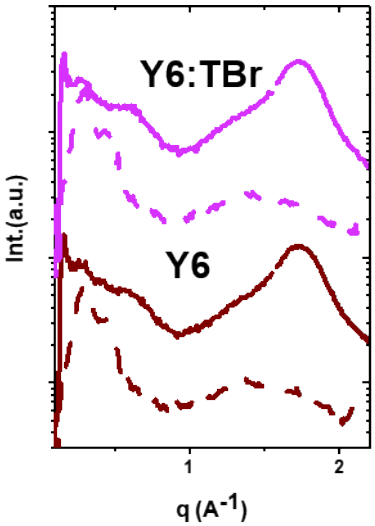

Figure S6. 1D profiles of Y6 and Y6:TBr 2D GIWAXS data taken along q_z (solid line) and q_{xy} (dash lins) axes.

Table S1. The OOP information of Y6 and Y6:TBr film

OOP direction	010 (Å^{-1})	FWHM (Å)	CCL (Å)	Intensity
Y6	1.74	0.30	18.6	24.6
Y6:TBr	1.74	0.28	20.0	25.7

Table S2. The IP information of Y6 and Y6:TBr film

IP direction	100 (Å^{-1})	FWHM (Å)	CCL (Å)	Intensity
Y6	0.26	0.097	57.6	50.8
Y6:TBr	0.26	0.093	60.0	63.7

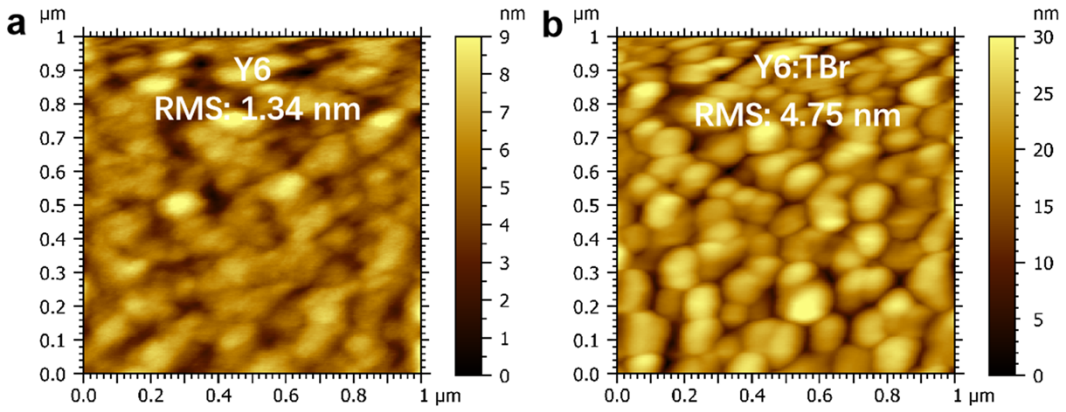

Figure S7. AFM surface topography images of Y6 and Y6:TBr films.

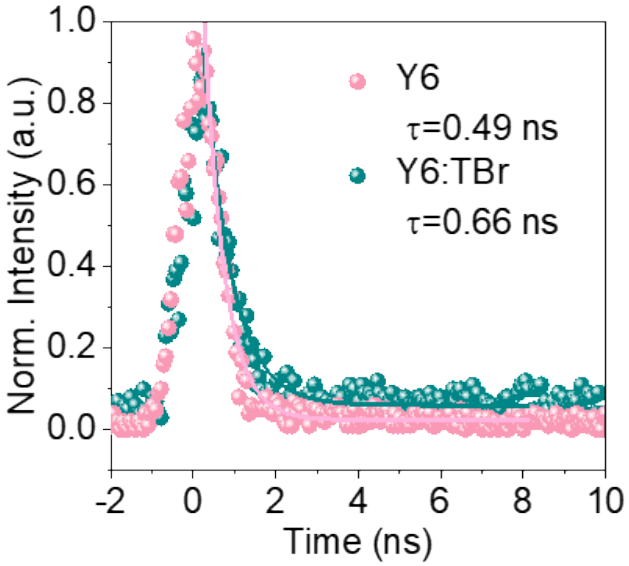

Figure S8. The TR-PL spectra of Y6 and Y6:TBr film.

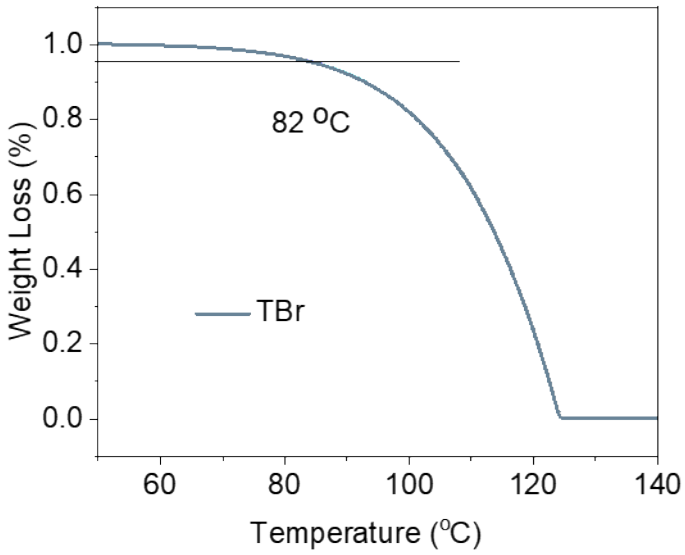

Figure S9. TGA curves of the TBr material.

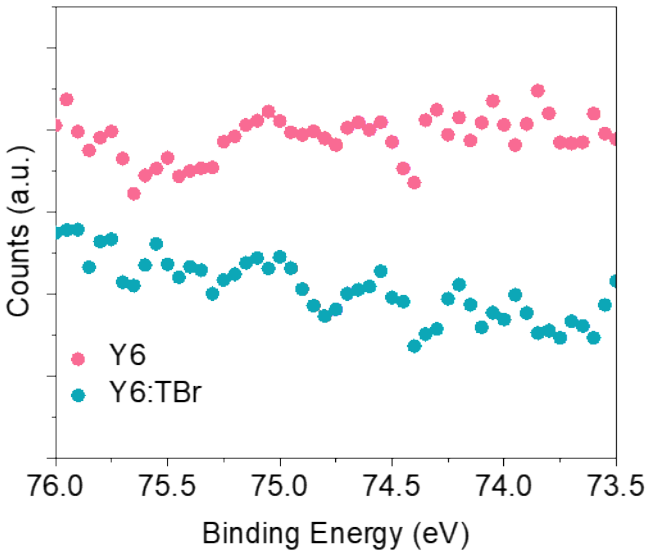

Figure S10. The XPS spectra of Br 3d for Y6 and Y6:TBr blend after thermal annealing at 85 °C for 5 mins.

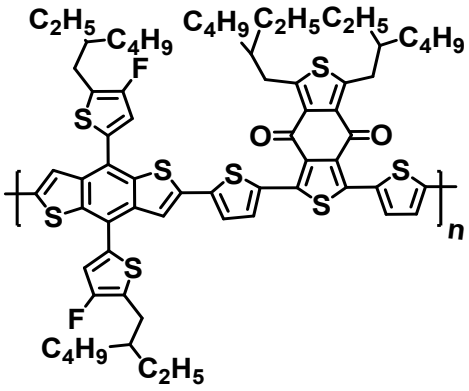

Figure S11. The chemical structure of PM6 polymer donor.

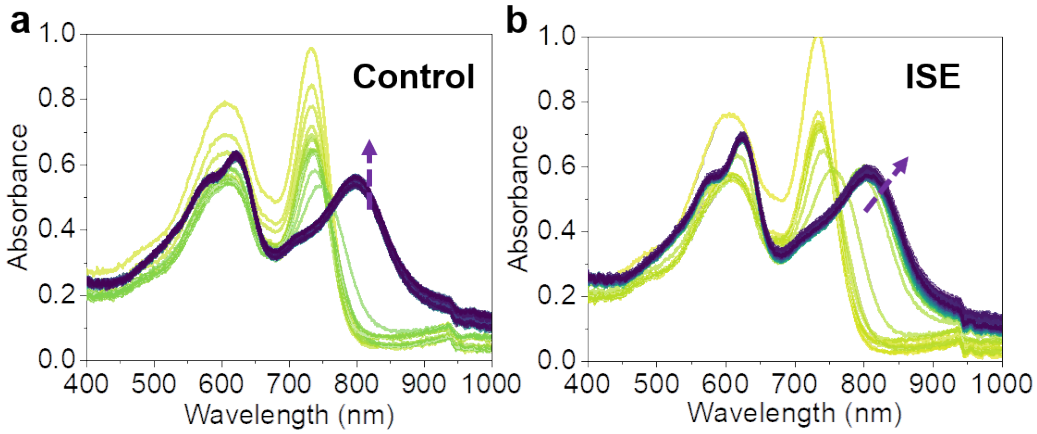

Figure S12. The time-resolved absorption curves for control (a) and ISE (b) blends.

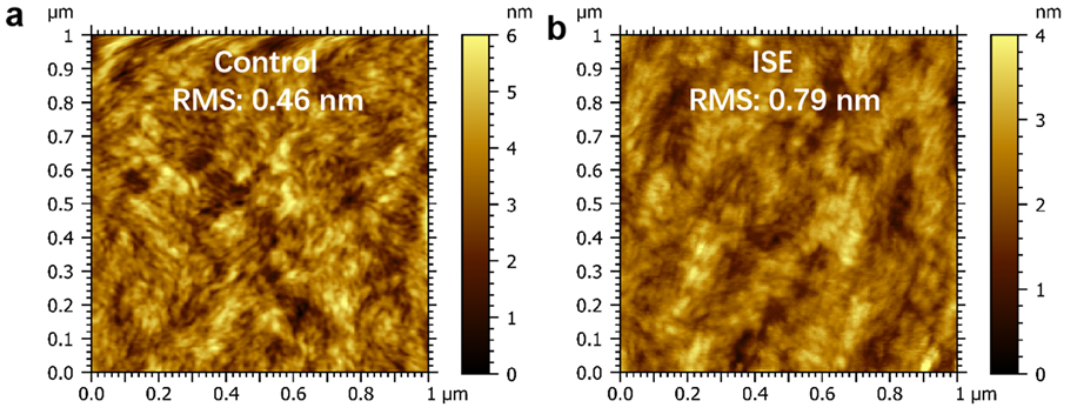

Figure S13. AFM images of control and ISE blend films.

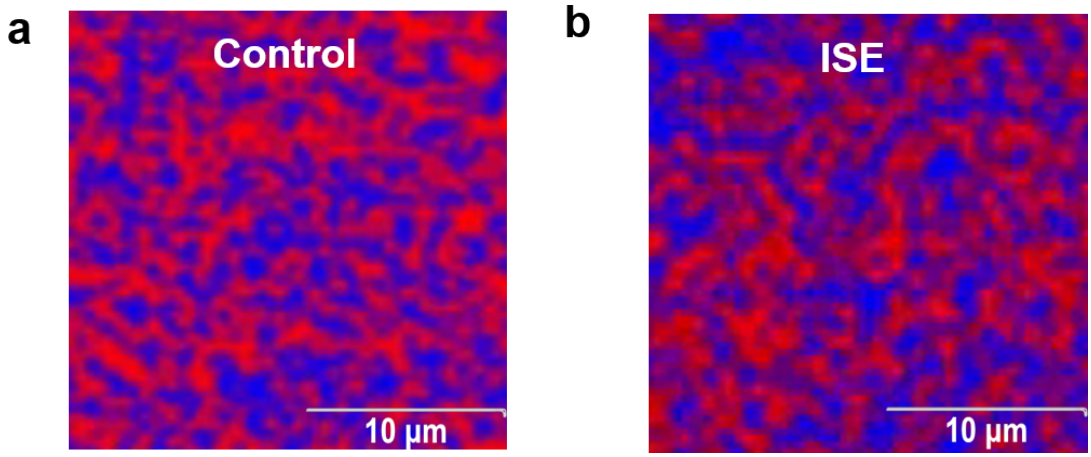

Figure S14. Raman mapping images of the PM6:Y6 BHJ active layers. The blue and red color regions represent the PM6 and Y6 domains in the BHJ blend films, respectively. PM6 possesses a characteristic Raman peak at 2955 cm^{-1}, and Y6 has a characteristic position at 2212 cm^{-1}.

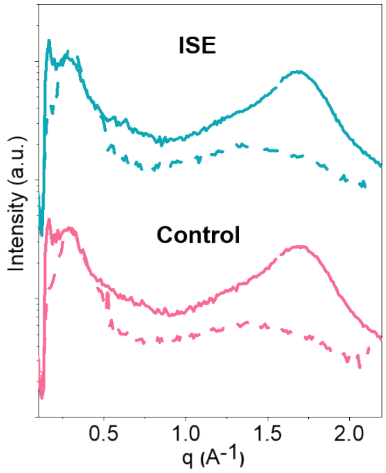

Figure S15. 1D profiles of control and ISE blend 2D GIWAXS data taken along q_z (solid line) and q_{xy} (dash lins) axes.

Table S3. The OOP information extracted from GIWAXS profiles

OOP direction	010 ($Å^{-1}$)	FWHM (Å)	CCL (Å)	Intensity
Control	1.70	0.31	18.0	17.1
ISE	1.69	0.30	18.6	18.7

Table S4. The IP information extracted from GIWAXS profiles

IP direction	100 ($Å^{-1}$)	FWHM (Å)	CCL (Å)	Intensity
Control	0.27	0.12	46.6	54.2
ISE	0.27	0.11	50.8	67.7

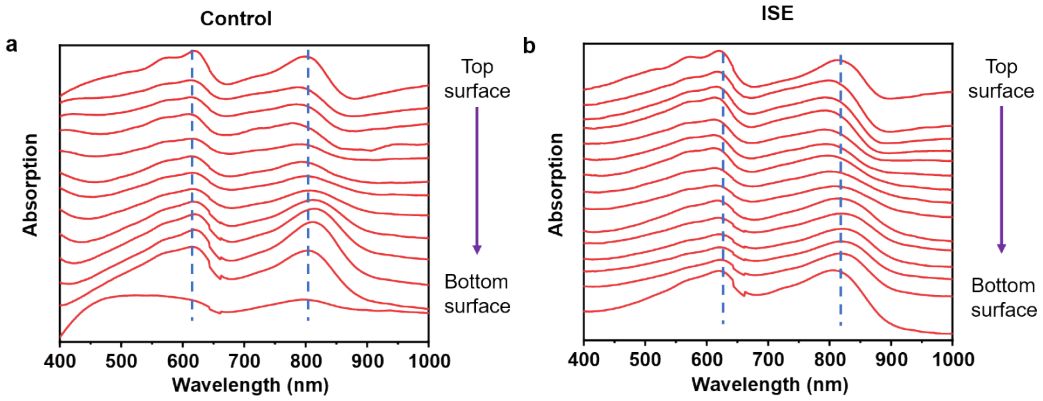

Figure S16. The UV-Vis absorption curves of control and TBr blend films as a function of etching thickness.

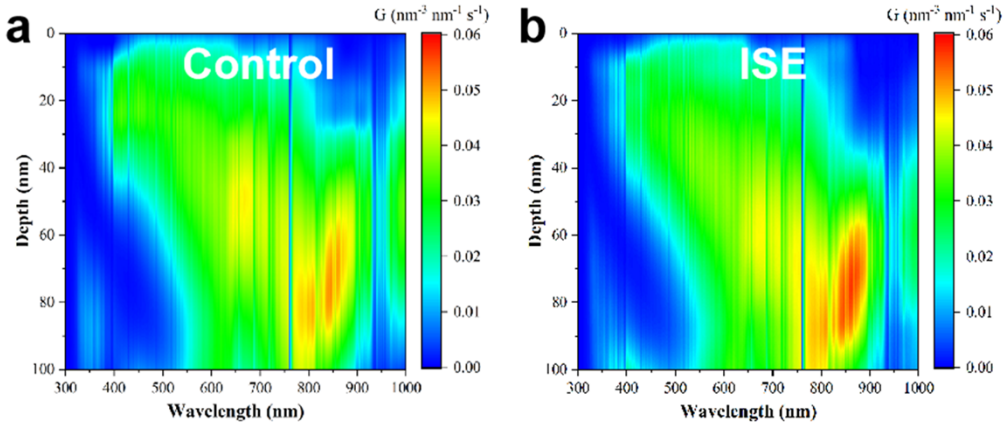

Figure S17. Exciton generation contours of control and ISE blend film as numerically simulated from the FLAS curves.

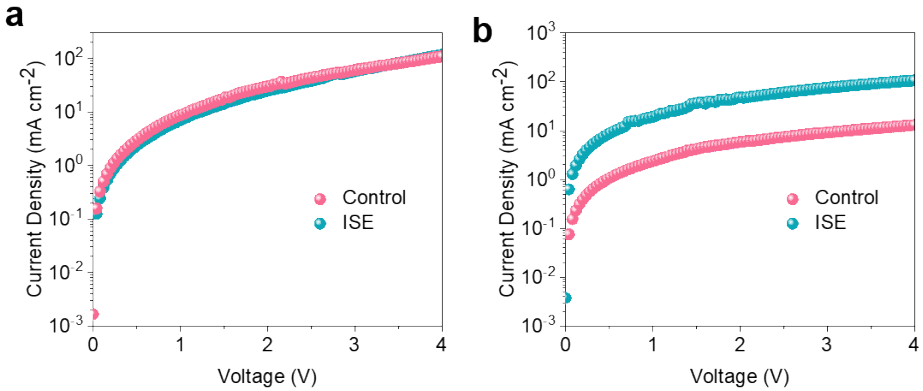

Figure S18. The (a) hole and (b) electron mobility for control and ISE blends extracted from hole-only devices and electron-only devices under dark conditions.

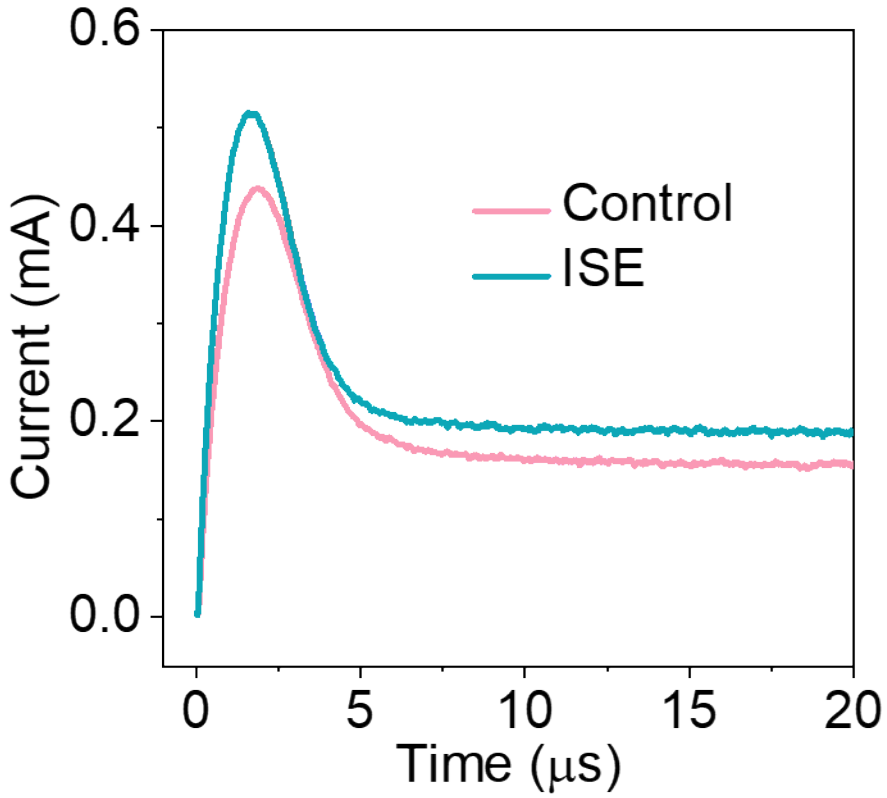

Figure S19. The Photo-CELIV curves of control and ISE devices.

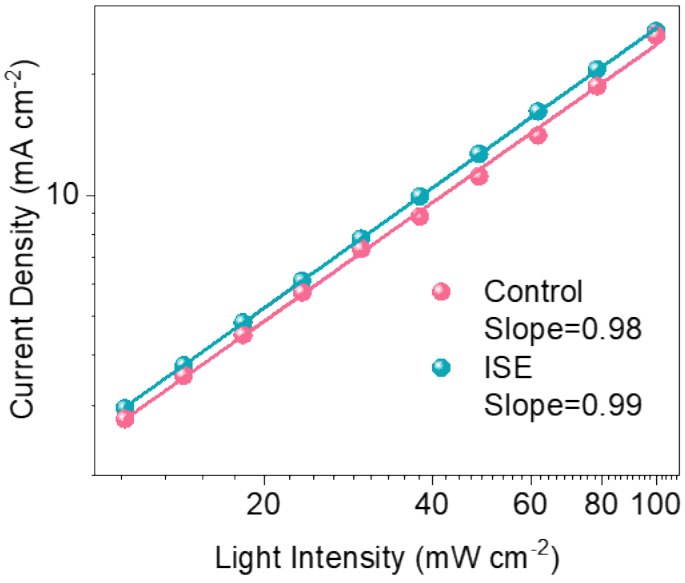

Figure S20. The dependence of J_{sc} on the light intensity in case of control and ISE treated devices. The relationship between the J_{sc} and light intensity can be described as $J_{sc} \propto I^{a}$, where I denotes the light intensity.

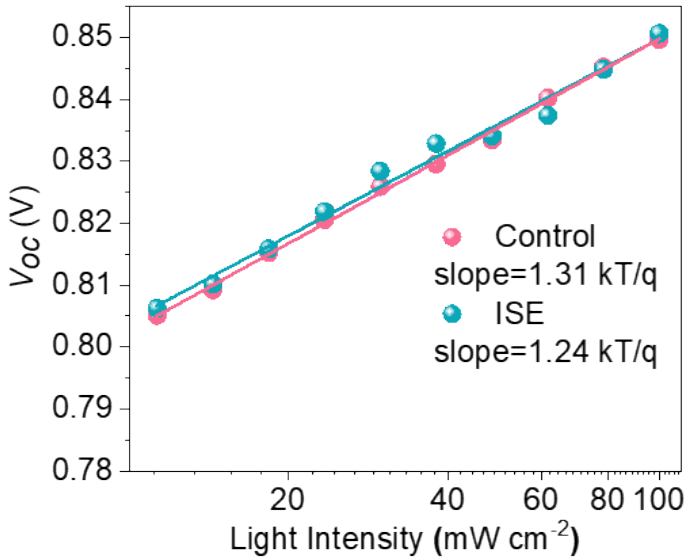

Figure S21. The dependence of V_{oc} on the light intensity in case of control and TBr treated devices. The correlation between V_{oc} as a function of I is a signal of trap-assisted recombination, which generally follows a natural logarithm relation $V_{oc} \propto \frac{nKT}{q} ln(I)$, where k, q and T represnet the Boltzmann constant, elementary charge and Kelvin temperature, respectively.

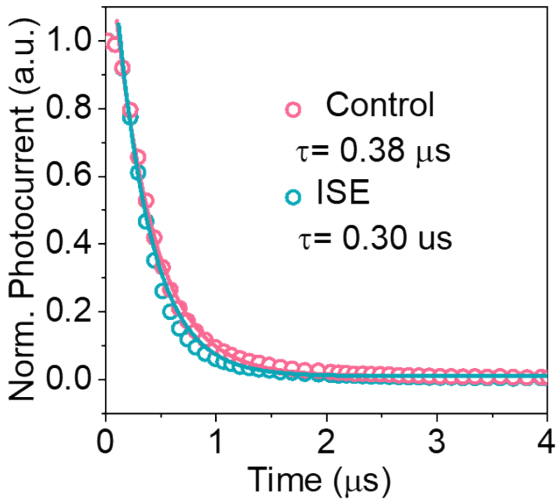

Figure S22. The TPC curves of control and ISE devices.

Table S5. Detailed device parameters of solar cells from the PM6:Y6 system with different amounts of TBr with 85 °C, 5min treatment.

PM6:Y6	V_{oc} (V)	J_{sc} (mAcm^{-2})	FF (%)	PCE$_{max}$ (%)
0 mg/ml	0.85	25.1	73.0	15.6
10 mg/ml	0.85	26.0	75.8	16.8
15 mg/ml	0.85	26.5	78.5	17.7
20 mg/ml	0.85	25.8	77.9	17.1
30 mg/ml	0.85	23.9	74.6	15.2

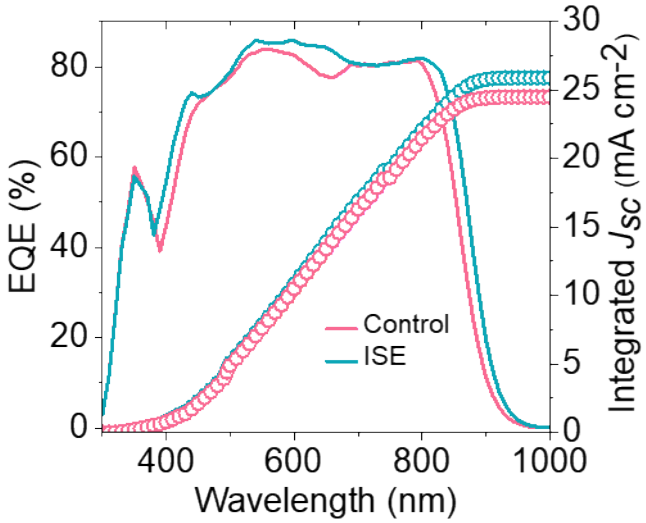

Figure S23. The EQE curves of control and ISE devices.

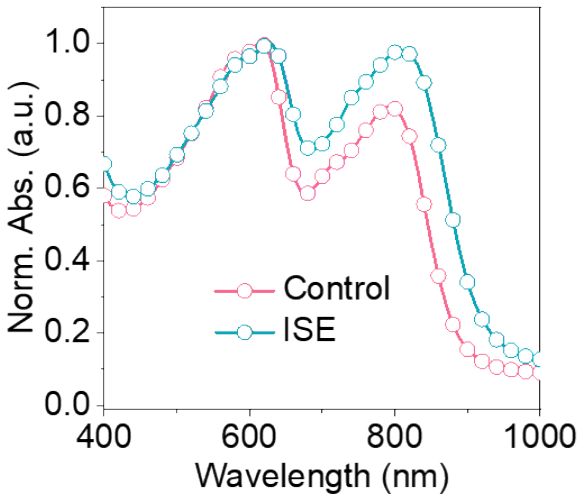

Figure S24. The UV-Vis absorption spectra of control and ISE blend, respectively.

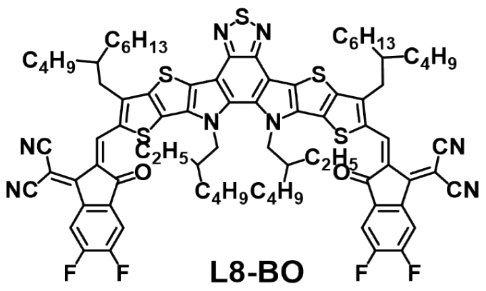

Figure S25. The chemical structure of L8-BO.

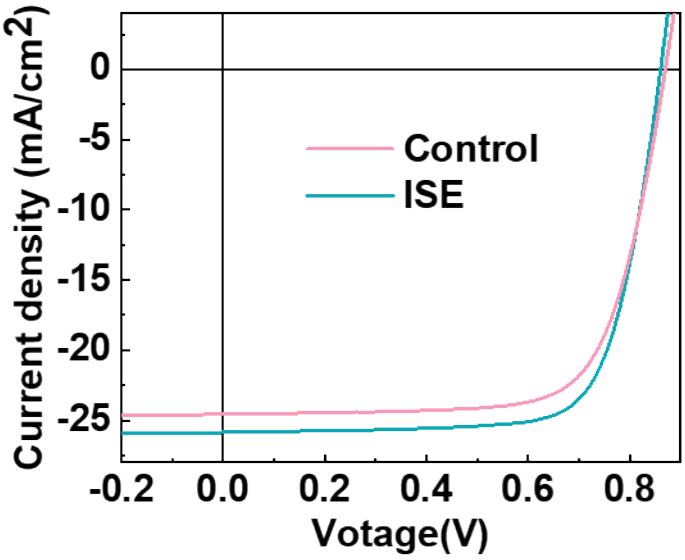

Figure S26. The *J-V* of control and ISE devices based on PM6:Y6-BO system.

Table S6. The performance parameter from the PM6:Y6-BO system with the addition of TBr (15 mg/ml). Average values with standard deviation were obtained from 10 devices.

PM6:Y6-BO	V_{oc} (V)	J_{sc} (mA cm^{-2})	FF (%)	PCE (%)
control	0.87 (0.86±0.01)	24.6 (23.7±0.9)	71.2 (68.4±3.9)	15.3 (15.0±0.4)
ISE	0.86 (0.85±0.01)	25.9 (25.0±1.0)	73.9 (70.3±3.1)	16.4 (16.0±0.4)

Table S7. The variation of thickness from the PM6:L8-BO system with the addition of TBr (15 mg/ml). Average values with standard deviation were obtained from 10 devices.

PM6:L8-BO	V_{oc}	J_{sc}	FF	PCE

	(V)	(mA cm^{-2})	(%)	(%)
100 nm	0.90 (0.90±0.01)	26.3 (25.7±0.5)	80.7 (78.5±2.6)	19.1 (18.7±0.3)
170 nm	0.90 (0.90±0.01)	26.3 (25.4±1.0)	77.6 (74.3±2.9)	18.6 (18.3±0.3)
240 nm	0.90 (0.90±0.01)	26.3 (25.6±0.9)	75.9 (71.0±3.8)	18.0 (17.6±0.4)
300 nm	0.90 (0.90±0.01)	26.5 (25.6±1.0)	74.5 (70.3±4.0)	17.8 (17.4±0.4)

Table S8. The summary of the photovoltaic performance of thick-film device in literature

No	Thickness[nm]	PCE[%]	Reference
1	460	11.47	*Adv. Energy Mater.* **2019**, *9*, 1902688
2	400	12.2	*Sol. RRL* **2020**, *4*, 2000476
3	320	12.6	*Chem. Eng. J.* **2021**, *405*, 127033
4	300	13.25	*Sol. RRL* **2021**, *5*, 2000787
5	300	15.28	*Adv. Funct. Mater.* **2022**, *32*, 2202103
6	300	15.5	*Adv. Mater.* **2022**, *34*, 2105114
7	300	15.9	*ACS Mater. Lett.* **2022**, *4*, 2009-2018
8	300	16.2	*Energy Environ. Sci.* **2021**, *14*, 6484-6493
9	300	16.61	*Adv. Funct. Mater.* 2022, 32, 2200807
10	300	17.0	*Adv. Mater.* **2022**, 34, 2200907
11	300	17.31	*Nat. Commtn.* **2022**, 13, 2369
12	330	17.46	*Adv. Funct. Mater. DOI: 10.1002/adfm.202301108*
13	300	17.8	***This work***

Table S9. Detailed device parameters of solar cells based on doctor blade coating technique. Average values with standard deviation were obtained from 10 devices.

PM6:L8-BO	V_{oc} (V)	J_{sc} (mA cm^{-2})	FF (%)	PCE (%)
ISE	0.90 (0.90±0.01)	26.2 (24.3±2.0)	72.5 (69.5±2.8)	17.1 (16.6±0.4)
control	0.90 (0.85±0.01)	24.7 (20.3±4.5)	58.5 (70.6±3.0)	13.0 (12.0±1.0)

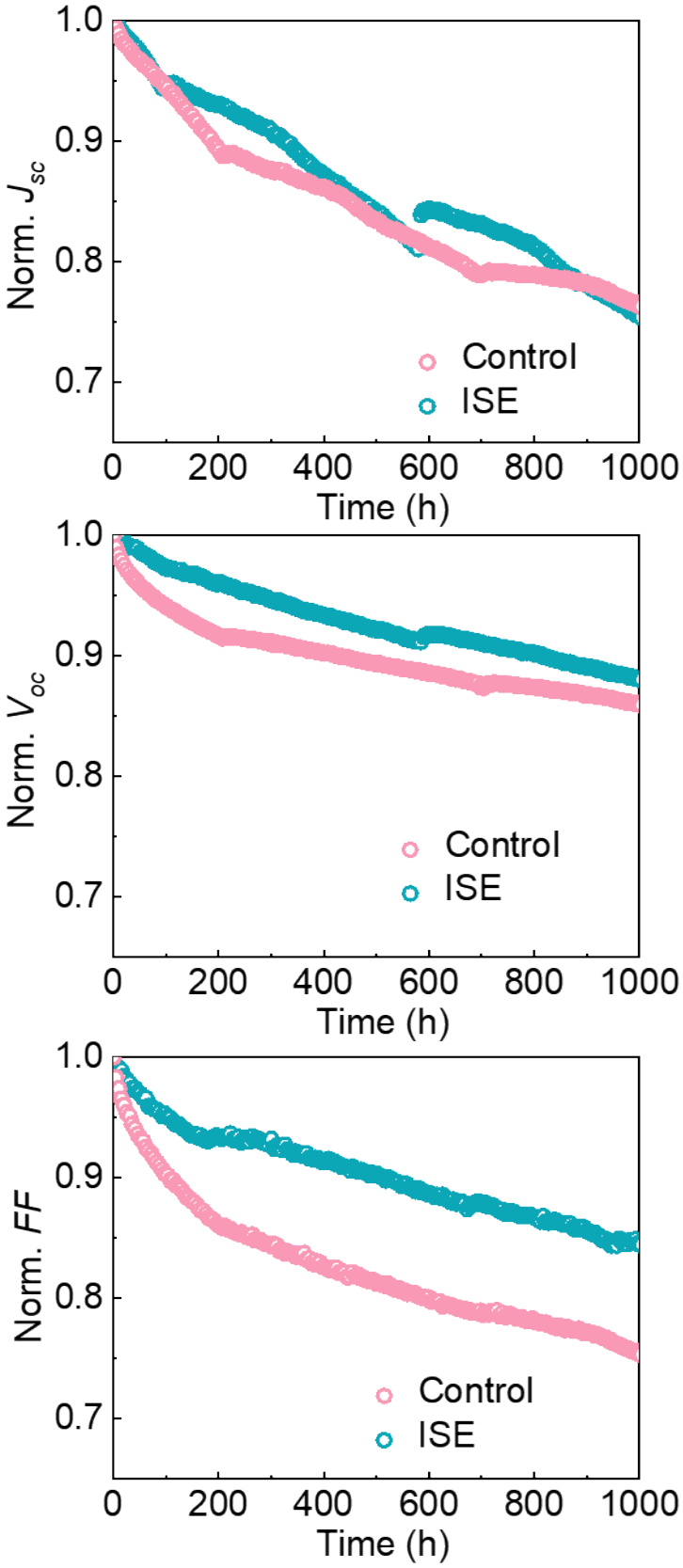

Figure S27. The normalized J_{sc}, V_{oc} and FF of control and ISE device under continuous AM 1.5 G 100 mW cm^{-2} condition.

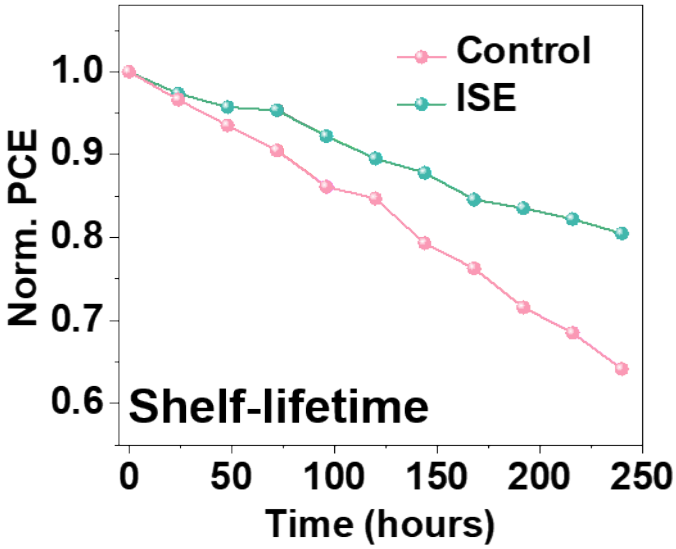

Figure S28. Normalized PCE of control and ISE devices under nitrogen-atmosphere in glove box.

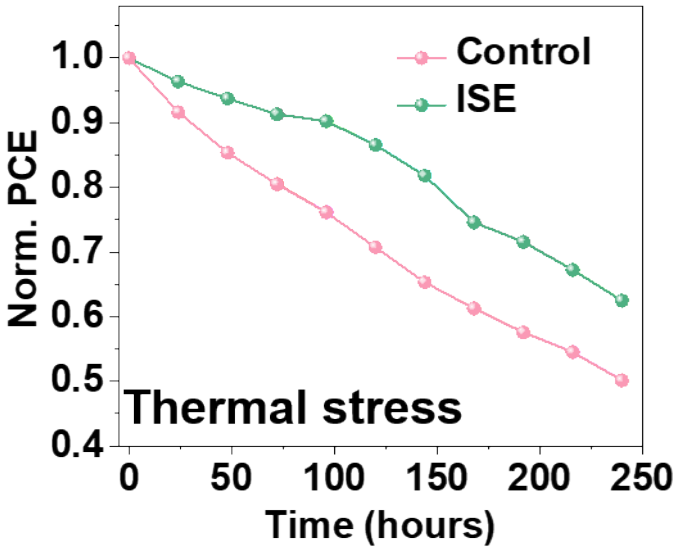

Figure S29. Normalized PCE of control and ISE devices under constant 65 °C thermal stress condition in glove box.